Accuracy of existing atomic potentials for the CdTe semiconductor compound

D. K. Ward,[1,a)] X. W. Zhou,[2] B. M. Wong,[3] F. P. Doty,[1] and J. A. Zimmerman[2]
[1]*Radiation and Nuclear Detection Materials and Analysis Department, Sandia National Laboratories, Livermore, California 94550, USA*
[2]*Mechanics of Materials Department, Sandia National Laboratories, Livermore, California 94550, USA*
[3]*Materials Chemistry Department, Sandia National Laboratories, Livermore, California 94550, USA*

(Received 15 March 2011; accepted 12 May 2011; published online 23 June 2011)

CdTe and CdTe-based $Cd_{1-x}Zn_xTe$ (CZT) alloys are important semiconductor compounds that are used in a variety of technologies including solar cells, radiation detectors, and medical imaging devices. Performance of such systems, however, is limited due to the propensity of nano- and micro-scale defects that form during crystal growth and manufacturing processes. Molecular dynamics simulations offer an effective approach to study the formation and interaction of atomic scale defects in these crystals, and provide insight on how to minimize their concentrations. The success of such a modeling effort relies on the accuracy and transferability of the underlying interatomic potential used in simulations. Such a potential must not only predict a correct trend of structures and energies of a variety of elemental and compound lattices, defects, and surfaces but also capture correct melting behavior and should be capable of simulating crystalline growth during vapor deposition as these processes sample a variety of local configurations. In this paper, we perform a detailed evaluation of the performance of two literature potentials for CdTe, one having the Stillinger-Weber form and the other possessing the Tersoff form. We examine simulations of structures and the corresponding energies of a variety of elemental and compound lattices, defects, and surfaces compared to those obtained from *ab initio* calculations and experiments. We also perform melting temperature calculations and vapor deposition simulations. Our calculations show that the Stillinger-Weber parameterization produces the correct lowest energy structure. This potential, however, is not sufficiently transferrable for defect studies. Origins of the problems of these potentials are discussed and insights leading to the development of a more transferrable potential suitable for molecular dynamics simulations of defects in CdTe crystals are provided. © *2011 American Institute of Physics*. [doi:10.1063/1.3596746]

I. INTRODUCTION

CdTe and CdTe-based $Cd_{1-x}Zn_xTe$ (CZT) alloys have engendered intensive research due to their numerous important applications. Thin films of CdTe are commonly used in solar cells[1,2] due to their impressive electronic properties (e.g., high solar energy absorption coefficient, optimal band gap for photoelectric conversation under solar radiation[3–5]), ease of manufacture, and low production cost as compared with other photovoltaic materials.[6,7] CdTe and CZT have also been the dominant semiconductors for radiation detection and medical imaging applications.[8–14] These materials have many attractive properties including high atomic numbers for efficient radiation-atomic interactions, and ideal band gaps for both a high electron-hole creation and a low leakage current. Despite the successful uses of CdTe and CZT, the material properties achieved today are still far from optimum. In the solar cell application, for instance, the current record energy conversion efficiency is only about 16% as compared with the theoretical prediction of 29% .[3,15–17] The difference has been attributed to various micro/nano scale charge-trapping defects in the multilayered films.[5,7,15,18–23] In the radiation detection application, property non-uniformity has been the limiting factor for both device performance and material cost (arising from a low yield of usable ingot portions).[8] Micron-scale defects such as grain boundaries and tellurium inclusions/precipitates have been known to affect carrier transport and uniformity by creating non-uniform charge trapping and electric fields.[8,24,25] Past efforts on minimizing these micron defects have not resolved the uniformity problem. Smaller scale defects such as dislocations[26] can also cause non-uniformity. Dislocations and tellurium precipitates both were found to decorate grain boundaries[8] and hence dislocations can be the root cause for non-uniformity by serving as the nucleation sites for tellurium precipitates. Unfortunately, the small scale defects have not been well studied in the past and were not considered in the material optimization.

CdTe or CZT are both soft (possessing a low yield strength) and brittle (possessing a low cleavage strength) which facilitates the creation of defects during the growth and manufacturing process.[14,27–35] It is therefore challenging to control defect formation using the experimental trial-and-error approach alone especially for nanoscale defects. Theoretical understanding of the effects and formation mechanisms of defects can play a critical role in material improvement. Various simulation techniques can be used

a)Author to whom correspondence should be addressed. Electronic mail: donward@sandia.gov.

to study the problem, including molecular dynamics (MD) (Refs. 36–38) and Monte Carlo (MC) methods,[39,40] where energies and forces can be determined from either density functional theory (DFT) (Refs. 41–43) or empirically constructed interatomic potentials.[36–38] In particular, MD with interatomic potentials provides an effective means to study the atomic scale structures at a length scale challenging for treatment by DFT-based MD and a detail of non-equilibrium conditions and structures unreachable by interatomic potential-based MC. With atomic configurations far from the equilibrium bulk lattice encountered during defect evolution under thermomechanical loading conditions, the key to having high fidelity MD simulations of defects is the use of a highly transferrable interatomic potential. Such a potential must not only capture a correct trend of structures and energies for a variety of elemental and compound lattices, defects, and surfaces, but also correctly reproduce the melting behavior and crystalline growth during vapor deposition, as these processes sample a variety of local configurations.

A literature survey indicates that there are two CdTe interatomic potentials already developed, one[40] is based upon the Stillinger-Weber format[44] (noted as SW potential), and the other one[36] is a Rockett modification[36,45] of the Tersoff potential[46] (noted as TR potential) (see Appendix A for their formalisms). The objective of this paper is to assess the applicability of these two potentials for MD studies of defect interaction and defect formation under thermomechanical conditions and identify a method to improve upon these models. This is done by comparing simulations of a variety of elemental and compound lattices, defects, and surfaces performed using the two potentials against those from experiments and/or *ab initio* calculations. The suitability of the potentials for disturbed configurations is also tested using melting temperature calculations and vapor deposition simulations. Insights that lead to a better model are then discussed.

II. COHESIVE ENERGY AND ATOMIC VOLUME

A useful way to assess the transferability of a CdTe interatomic potential is to calculate the atomic volume and cohesive energy of various Cd, Te, and CdTe clusters and phases with coordination from 1 to 12 and to compare these to the corresponding data from experiments and density functional theory (DFT) calculations. This is especially important in understanding Te precipitates. Studies have shown that the secondary Te structure depends on growth conditions and can range from a high pressure rhombohedral phase,[27] a normal trigonal phase,[28] an amorphous phase,[28] an hcp representation of the trigonal phase,[29] and a monoclinic phase. After considering a larger structure basis based on our experiences,[47] our choice of clusters and crystal phases are as follows:

- For pure Cd, we study dimer (di), trimer (tri), square (sq), tetrahedron (tetra), and four-atom-chain (ch) clusters and diamond-cubic (dc), simple-cubic (sc), body-centered-cubic (bcc), face-centered-cubic (fcc), hexagonal-close-packed (hcp), graphite (gra), and graphene (grap) lattices.
- For pure Te, we study the same cluster and lattice types listed above for Cd, plus the γ-Se (A8) lattice.
- For the Cd-Te binary system, we study the zinc-blende (zb), wurtzite (wz), NaCl (B1), CsCl (B2), and binary-graphene (grap) lattices for the stoichiometric compound CdTe, plus two non-stoichiometric trimers, Cd_2Te, and $CdTe_2$.

Experiments indicated that equilibrium phases for Cd, Te, and CdTe are hcp, A8, and zb (Ref. 48) with atomic volumes of 21.46 Å^3/atom, 33.76 Å^3/atom, and 33.98 Å^3/atom, respectively. The experimental cohesive energies derived from the thermochemical data[49] are –1.133 eV/atom, –2.168 eV/atom, and –2.178 eV/atom for the three equilibrium phases. DFT calculations are used to calculate structures and energies for non-equilibrium, metastable phases not observed in experiments (see Appendix B). While DFT calculates energy differences between different phases well, it does not yield accurate absolute energies. Thus, the DFT energies should only be considered as a relative measure between phases and trends.

Based on the CdTe Stillinger-Weber and Tersoff-Rockett potentials, molecular statics (energy minimization) simulations were performed to calculate the relaxed structures and energies of the different phases. Large-scale Atomic/Molecular Massively Parallel Simulator (LAMMPS) (Ref. 50) was used for the energy minimizations. The simulations used a Polak-Ribiere conjugate gradient method, with a stopping energy tolerance of 10^{-12} eV, and a stopping force tolerance of 10^{-14} eV/Å, and were performed under a zero pressure condition using the method developed by Parrinello and Rahman.[51]

A. Cohesive energy

The calculated cohesive energies using the two potentials were determined using the molecular statics method. Figure 1 shows a comparison of the calculated data for selected important crystalline structures with those obtained from

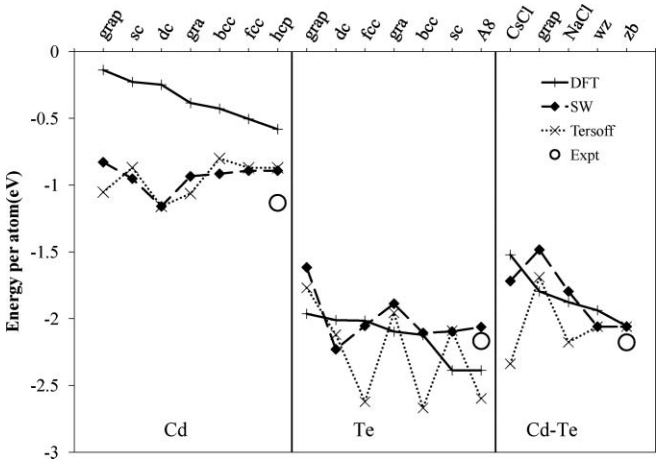

FIG. 1. Energies of various Cd, Te, and CdTe phases computed using DFT, SW, and TR.

DFT calculations and experiments.[49] A sizeable discrepancy between DFT and experimental values can be seen in the cohesive energy of the Cd hcp structure. This energetic difference arises from the lack of dispersion interactions in conventional DFT functionals which, in the case of cohesive energies, can play a large role in energetic stability.[52,53] The incorporation of dispersion effects beyond the single-particle DFT approach would require significant modifications to our code (in addition to significant computational effort), and will be addressed in future work.[89] The energy trends of different phases predicted by the SW and the TR potentials are both substantially different from that determined by the DFT method. Most seriously, both SW and TR potentials have a dc lowest energy Cd structure, whereas DFT and experiments show that the lowest energy phase should be hcp. This means that the SW and TR cannot be used to model Cd. Similarly, the SW and TR potentials incorrectly have a dc structure and bcc structure as the lowest energy for Te, respectively. DFT and experiments indicated that the A8 structure should have the lowest energy. Although the cohesive energy of the A8 Te structure predicted by the TR potential is not significantly higher than that of the bcc Te structure, the TR potential gives the worst energy trend across different phases as it essentially predicted three "lowest" energy Te phases of fcc, bcc, and A8 with energies significantly lower than the corresponding phases calculated using the DFT method. Hence, the SW and TR potentials are not suitable for modeling Te. The observation that the SW and TR potentials cannot model Cd and Te can be understood because many of the potential parameters are set to those of Si as discussed in Appendix A.

The SW and TR potentials were fit using CdTe zb data with a cohesive energy of –2.06 eV/atom. In fact, the experimental cohesive energy of zb CdTe is –2.178 eV/atom.[54] But of greater importance are the energy trends between structures. For the SW potential, the energy trend shown in Fig. 1, while not ideal, has some similarities to that of DFT. Most importantly, it does give the zb structure as the lowest energy phase. As a result, the SW potential at least allows MD simulations of the zb CdTe structure. A serious problem is seen for the TR potential, as it not only has a structure energy trend significantly different from that of DFT, it also has NaCl (B1) and CsCl (B2) (shown in Fig. 1) as lower energy structures relative to zb. This means that the TR potential may not even permit stable MD simulations of the zb CdTe especially under thermomechanical conditions where phase transformation may be triggered. Note that the problem was revealed by exploring only a limited number of phases. A much more stringent test is simulating vapor deposition where many local configurations not represented by the phases explored here will be encountered (see Sec. VII).

In addition to the cohesive energies for crystal structures, the calculations of various clusters are compared to DFT and experimental values, shown in Table I. Interestingly, both potentials over predict (larger magnitude) the Cd cluster energies and under predict the Te cluster energies. Both potentials also over predict the three CdTe cluster energies. These large differences can greatly influence the thermodynamics of the system.

TABLE I. Cd-Te cluster energies (eV).

	Experiment	DFT	SW	TR
Cd dimer	–0.04[a]	–0.06	–0.58	–0.72
Cd trimer	…	–0.21	–1.05	–1.00
Cd square	…	–0.24	–2.11	–2.07
Cd rhombus	…	–0.32	–2.11	–2.07
4 Cd linear chain	…	–0.20	–1.38	–1.93
Cd tetrahedron	…	–0.56	–1.53	–1.40
Te dimer	–2.66[b]	–3.43	–1.12	–1.20
Te trimer	…	–5.67	–2.29	–2.29
Te square	…	–7.63	–4.18	–4.00
Te rhombus	…	–7.63	–4.18	–4.00
4 Te linear chain	…	–7.05	–1.38	–1.93
Te tetrahedron	…	Unstable	–3.46	–3.60
CdTe dimer	…	–0.17	–1.03	–1.14
TeCdTe trimer	…	–3.45	–2.09	–2.32
CdTeCd trimer	…	–1.53	–2.06	–2.29

[a]Data from Barin *et al.* (Ref. 92).
[b]Data from Viswanathan *et al.* (Ref. 93).

B. Atomic volumes and bond lengths

The atomic volumes calculated using the SW and TR potentials are compared with the DFT calculations and the experimental data in Fig. 2 for important structures. As for energies, the trends between phases are a more important measure than the actual volumes. The overall trend of the atomic volumes of the two potentials roughly follows that of DFT, but some exceptions occur. In particular, large jumps in the volume trends which are either predicted by DFT and not by the potentials or vice versa are highly undesirable. A more suitable trend would have a potential that could be adjusted according to the arrows shown in the Fig. 2.

Since atomic volumes are not well defined for the small clusters, the bond lengths for the structures are compared in Table II. The SW and TR potentials over estimate the bond lengths for the Cd tetrahedron bond lengths by 7% and 4%, respectively. The remaining Cd cluster bond lengths are all underestimated by 3%–15% for the SW and 6%–17% for the

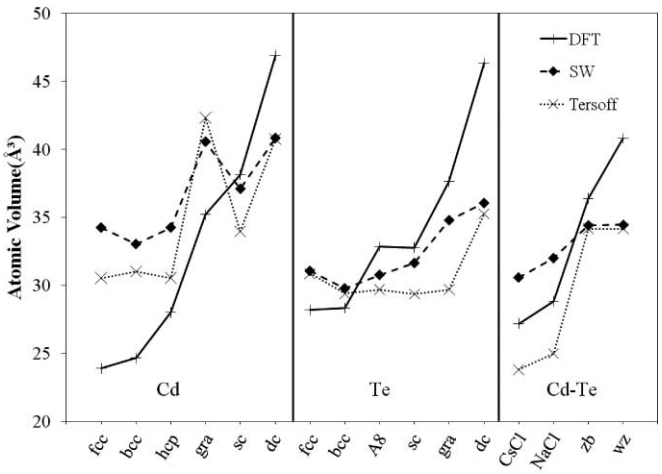

FIG. 2. Atomic volumes of different Cd, Te, and CdTe phases computed using DFT, SW, and TR. Arrows indicate points that should be adjusted in order to capture correct trends.

TABLE II. Cd-Te cluster bond lengths (Å).

	Experiment	DFT	SW	TR
Cd dimer	4.07[a]	3.50	2.98	2.92
Cd trimer	...	3.38	3.28	3.18
Cd square	...	3.53	3.04	3.01
Cd rhombus	...	3.51	3.04	3.01
4 Cd linear chain[b]	...	3.44, 3.39	3.07, 3.25	2.94, 2.96
Cd tetrahedron	...	3.22	3.44	3.33
Te dimer	2.56[c]	2.58	2.86	2.78
Te trimer	...	2.76	3.11	3.01
Te square	...	2.80	2.90	2.86
Te rhombus	...	2.80	2.90	2.86
4 Te linear chain[b]	...	2.60, 2.83	3.07, 3.25	2.94, 2.97
CdTe dimer	...	2.57	2.82	2.77
TeCdTe trimer[d]	...	4.12,2.57	3.12, 3.09	2.91, 3.01
CdTeCd trimer[d]	...	2.82, 2.88	2.82, 4.60	2.77, 4.96

[a]Data from Lukeš *et al.* (Ref. 94).
[b]For the 4 member linear chains, the first value is the bond length between the outer most atom and its neighbor. The second value is the bond length between the two inner atoms.
[c]Data from Hube *et al.* (Ref. 95).
[d]For the ABA trimer, the first value is the AB bond length and the second value is the AA bond length.

TR. In contrast to the Cd clusters, both potentials over predict all of the Te cluster bond lengths: SW 3%–18% and TR 2%–13%. The two potentials really do a reasonable job for the Cd-Te dimer bond length with differences of 4% for SW and 3% for TR. For the CdTeCd trimer, both potentials do an excellent job reproducing the bond lengths between CdTe $\sim$ 0% (SW) and 2% (TR), but the distances between the two Cd atoms are greatly over predicted 60% (SW) and 72% (TR). For the TeCdTe trimer structures, the potentials under predicted the CdTe bond lengths by 24% (SW) and 30% (TR) and over predicted the TeTe bond length by 20% (SW) and 17% (TR).

III. ELASTIC CONSTANTS

Elastic constants are important properties to capture in the simulations as they affect the strain energy around defects and dislocation properties. The elastic properties of the CdTe zb as well as the bulk moduli for several of the elemental Cd and Te crystal structures have been calculated using MD simulations. The elastic constants were determined from the second derivatives of the energy with respect to strain $\partial^2 E/\partial\varepsilon_i\partial\varepsilon_j$, where E and ε_i ($i = 1, 2, \ldots, 6$) are, respectively, the energy and strain. The implementation of the method was verified as our SW calculations agree with those reported by Wang *et al.*[40] using an analytic technique for calculating elastic constants for a given potential.[55] Table III compares the elastic constants of the zb CdTe structure calculated from the SW and the TR potentials with the corresponding data obtained from DFT calculations and experiments. In Table III, c_{44}^0 and c_{44} represent the unrelaxed (homogeneously sheared crystal) and relaxed (a crystal allowed to relax between two sheared plates) shear modulus, respectively. The TR potential captures the elastic constants of the CdTe compound fairly well with only 5%–25% difference from the experimental values. The SW potential produces somewhat larger errors of about 17%–46% from experimental values.

TABLE III. Elastic constants of zinc-blende CdTe (GPa).

c_{ij}	Expt. (300 K)	DFT	TR	SW
c_{11}	53.3[a]	53.2[b]	50.7	44.3
c_{12}	36.5[a]	36.0 [b]	37.5	19.6
c_{44}	20.4[a]	...	15.2	18.0
$c_{44}^{(0)}$	...	31.8 [b]	46.8	30.7

[a]Data from Rowe *et al.* (Ref. 96).
[b]Data from Agrawal *et al.* (Ref. 41).

The bulk moduli of a variety of metastable Cd and Te phases have also been calculated. The bulk moduli for the two potentials are compared with DFT calculations and the available experimental data in Tables IV and V for the various Cd and Te phases. For the higher atomic volume structures (sc, dc, and gra), the moduli for the SW potential are, within 2%–8% for Cd and 15%–21% for Te, as compared to the TR potential, within 10%–139% for Cd and 17%–94% for Te. Yet for the low atomic volume structures (bcc, fcc, hcp, A8), the SW potential has unreasonably large moduli, 251%–263% larger for Cd and 295%–300% larger for Te, compared to the TR potential, 56%–80% and 7%–15% larger for Cd and Te, respectively. As will be discussed in more detail below, SW is only applicable for open (dc) structures and hence its poor prediction of elastic properties for closely packed structures is not surprising. When TR is not well parameterized, it may result in poor elastic properties especially since the Tersoff functions have non-continuous second derivatives at atomic spacings that may overlap with the second (or above) nearest neighbors.[56]

IV. POINT DEFECT ENERGETICS

In addition to Te inclusions and precipitates, native point defects such as vacancies, interstitials, and antisites (Cd atoms on Te sites and vice versa) are often seen in CdTe crystals. The primary native defects in CdTe compounds are Cd interstitials under the Cd-rich condition, and Cd vacancies, Te interstitials, and Te antisites[30,57] under the Te-rich conditions. All of these defects ultimately affect charge transfer properties of the material. Thus, an important aspect of the MD model is the capability to predict the presence and interactions of native defects in the zb CdTe. Various types of defects

TABLE IV. Bulk moduli of various Cd phases (GPa). Experimental value is in parentheses.

	DFT	TR	SW
sc	44.4	40.0	41.4
dc	18.9	45.1	19.2
gra	22.7	40.2	20.8
bcc	33.8	60.8	119.1
fcc	42.8	69.2	155.5
hcp	44.3 (62.2[a])	69.2	155.5

[a]Data from Béré *et al.* (Ref. 97).

TABLE V. Bulk moduli of various Te phases (GPa). Experimental value is in parentheses.

	DFT	TR	SW
sc	53.2	13.7	61.1
dc	27.4	22.8	31.7
gra	35.6	68.9	28.0
bcc	57.6	63.1	227.8
fcc	56.9	60.6	227.6
A8	51.6 (24[a])	59.3	203.6

[a]Data from Parthasarathy *et al.* (Ref. 98).

can be easily introduced in the computational crystal used in molecular dynamics or molecular statics calculations. The stoichiometry of the system containing the defects depends on the environment and it does not necessarily equal the stoichiometry of the perfect crystal. Following the methodology of Zhang and Northrup,[47,58,59] the defect energy Γ is calculated as a function of the chemical potential difference $\Delta\mu$ as

$$\Gamma = E_D^{'} - (n_{\mathrm{Cd}} - n_{\mathrm{Te}}) \cdot \Delta\mu, \tag{1}$$

where n_{Cd} and n_{Te} are numbers of Cd and Te atoms in the defective system, $\Delta\mu$ is the chemical potential difference characteristic of the environment, and $E_D^{'}$ is the intrinsic defect energy at stoichiometric condition. $\Delta\mu$ is expressed as

$$\Delta\mu = \left(\mu_{\mathrm{Cd}} - \mu_{\mathrm{Cd}}^{\mathrm{bulk}}\right) - \left(\mu_{\mathrm{Te}} - \mu_{\mathrm{Te}}^{\mathrm{bulk}}\right), \tag{2}$$

where μ_{Cd} and μ_{Te} are the chemical potentials of Cd and Te in the CdTe compound, and $\mu_{\mathrm{Cd}}^{\mathrm{bulk}}$ and $\mu_{\mathrm{Te}}^{\mathrm{bulk}}$ are the chemical potentials (approximated here as cohesive energies per formula unit) for the lowest energy Cd and Te phases. $\Delta\mu$ satisfies the condition $-\Delta H_f < \Delta\mu < \Delta H_f$ where ΔH_f is the heat of mixing.[59] In general, $\Delta\mu = 0$, $\Delta\mu > 0$, and $\Delta\mu < 0$ mean stoichiometric, Cd-rich, and Te-rich conditions. In the MD simulations performed here, $\Delta\mu$ is left as an independent adjustable variable for the Cd and Te-rich environments.

The intrinsic defect energy can be calculated as

$$E_D^{'} = E_D - (n_{\mathrm{Cd}} + n_{\mathrm{Te}}) \cdot \mu_{\mathrm{CdTe}}^{\mathrm{bulk}} - (n_{\mathrm{Cd}} - n_{\mathrm{Te}}) \cdot \left(\mu_{\mathrm{Cd}}^{\mathrm{bulk}} - \mu_{\mathrm{Te}}^{\mathrm{bulk}}\right), \tag{3}$$

where E_D is the total energy of the system containing the defect and $\mu_{\mathrm{CdTe}}^{\mathrm{bulk}}$ the chemical potential (approximated as the cohesive energy) of the lowest energy CdTe phase.

The defects considered include Cd vacancy (V_{Cd}), Te vacancy (V_{Te}), Cd at Te antisite (Cd_{Te}), Te at Cd antisite (Te_{Cd}), Cd interstitial surrounded by the Cd tetrahedron shell (Cd_{i1}), Cd interstitial surrounded by the Te tetrahedron shell (Cd_{i2}), Te interstitial surrounded by the Cd tetrahedron shell (Te_{i1}), and Te interstitial surrounded by the Te tetrahedron shell (Te_{i2}). Molecular statics simulations were performed to calculate the minimized total energies of the systems containing the corresponding defects, E_D, and the intrinsic defect energies were calculated under stoichiometric conditions ($\Delta\mu = 0$) for which Eq. (1) reduces to Eq. (3). Similar calculations were performed using DFT with computational details described in Appendix B. The results obtained from the potentials and DFT are compared in Table VI.

TABLE VI. Defect energies for zinc-blende CdTe (eV). DFT values include results calculated here and results from Wei *et al.* (in parantheses) for Ref. 33

	DFT	SW	TR
Cd vacancy, V_{Cd}	2.20 (2.67)	2.60	2.43
Te vacancy, V_{Te}	2.72 (3.24)	1.53	0.93
Cd antisite, Cd_{Te}	3.01 (3.92)	0.80	0.18
Te antisite, Te_{Cd}	3.16 (3.70)	0.74	1.19
Cd interstitial 1, Cd_{i1}	1.98 (2.04)	4.27	1.36
Te interstitial 1, Te_{i1}	3.52 (3.41)	2.60	0.55
Cd interstitial 2, Cd_{i2}	2.14 (2.26)	3.76	0.61
Te interstitial 2, Te_{i2}	3.91 (3.52)	3.57	1.28

Table VI reveals that the defect energies calculated by the two potentials deviate from the DFT results quite significantly. Most importantly, the SW potentials indicate that under the stoichiometric condition, the Cd_{Te} and Te_{Cd} antisites have very low energies (0.74–0.80 eV). Contrarily, DFT determined that these two defects have high energies (3.01–3.16 eV). Worse than the SW potential, the TR potential indicated that the intrinsic defect energy for the Cd_{Te} antisite is only 0.18 eV, further contradicting the DFT results. The TR potentials also showed that the Te_{i1} and Cd_{i2} interstitials have low defect energies (0.55–0.61 eV), whereas DFT results showed that these two defects have fairly high energies (2.14–3.52 eV). Note that SW and TR results are all based on incorrect lowest energy structures of the elemental phases. This analysis suggests that the SW and the TR potentials do not sufficiently capture the defect properties and should not be used to study defects.

V. SURFACE RECONSTRUCTIONS

Simulations of mechanical processes, such as fracture, and growth processes, such as vapor deposition, require accurately reproducing surface structures and energies. The (001) surface of the zb CdTe crystal has exhibited a variety of surface reconstructions depending on the environment.[60–62] Some possible surface reconstructions, as reported by Gundel *et al.*[43] are shown in Fig. 3. Using DFT simulations, Gundel *et al.*[43] predicted that for Te-rich environments, the Te (2×1) coverage $\theta = 1.0$ reconstruction was favorable, whereas for Cd-rich environments, the Cd c(2×2) coverage $\theta = 0.5$ is the favorable reconstruction. Their simulation is consistent with experiments where Tatarenko *et al*. reported a Te (2×1) (Ref. 63) in Te-rich environments and Seehofer *et al*. reported a Cd c(2×2) surface in Cd-rich environments.[60]

Following previous work,[47,64] the energies of different surface reconstructions were calculated as a function of the same chemical potential difference as defined in Eq. (2). All of the 10 Cd-Te (001) surface reconstructions shown in Fig. 3 were simulated. The computational cell used in each simulation contained a block of zb CdTe crystal with ~2300–2500 atoms. Periodic boundary conditions were used in the x and y directions and two parallel free surfaces (with the same reconstructions) were created in the ± z directions. The two surfaces were not perfectly symmetric as one of the free

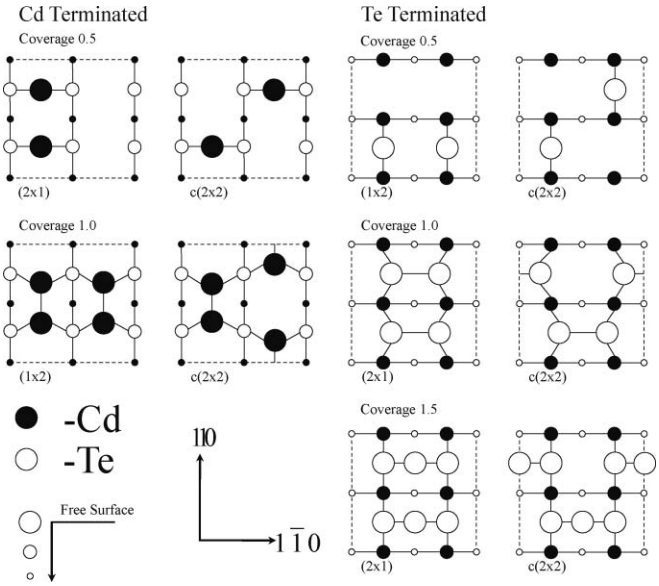

FIG. 3. Surface reconstructions for (100) zinc-blende CdTe (see Ref. 43).

surfaces was rotated 90° relative to the opposite face. The results are summarized in Figs. 4 and 5 for the SW and TR potentials, respectively. Figure 4 indicates that within the possible range of chemical potential difference between $-\Delta H_f$ and ΔH_f, the preferred surface for the SW potential is Te (2×1) coverage $\theta = 1.0$ in the Te-rich environments ($\Delta\mu$ at the $-\Delta H_f$ end) and Cd (1×2) coverage $\theta = 1.0$ in the Cd-rich environments ($\Delta\mu$ at the ΔH_f end). Figure 5 indicates that the TR potential, on the other hand, has Cd (1×2) coverage $\theta = 1.0$ and Cd c(2×2) coverage $\theta = 1.0$ surfaces as the two most favorable reconstructions under all chemical potential conditions $-\Delta H_f < \Delta\mu < \Delta H_f$.

Figures 4 and 5 indicate that the energies of all the surfaces with the 0.5 coverage are independent of the chemical potential. This is because the numbers of atoms of the two species in the system are equal when the surface stoichiometry is 50/50. DFT results from Gundel *et al.*[43] showed the Te 0.5 coverage surfaces have an energy ~0.2 eV/(1×1 cell) higher than the Cd 0.5 coverage surfaces. Contrarily, Figs. 4 and 5 indicate that the energies of surfaces with the 0.5 coverage are indistinguishable. It can be seen from Fig. 3 that all surfaces with the 0.5 coverage are bulk terminated. As a result, it is not surprising that potentials considering only the nearest interactions cannot distinguish these surfaces. On the other hand, if the surfaces are not bulk terminated but rather the surface atoms are dimerized, the potentials will give different energies.

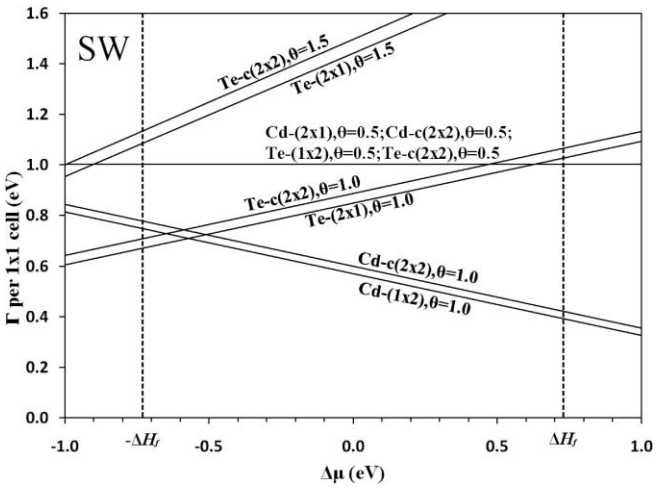

FIG. 4. Surface energies of (001) zinc-blende CdTe surfaces as a function of chemical potential difference calculated by SW.

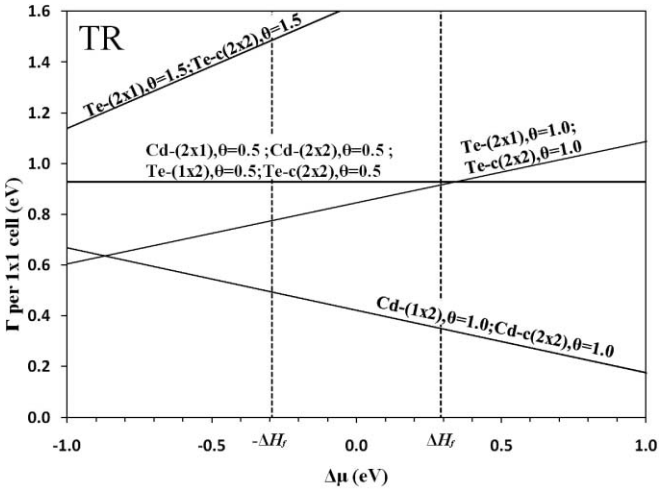

FIG. 5. Surface energies of (001) zinc-blend CdTe surfaces as a function of chemical potential difference calculated by TR.

VI. MELTING TEMPERATURE

Reproducing the correct melting properties of a material can serve as an important validation of an atomistic model because a variety of local configurations can be sampled during a melting process. MD simulations were performed to calculate the melting temperatures, and LAMMPS was used for the simulations. The equations of motion were integrated using the Verlet integrators of Tuckerman *et al.*[65] at a time step of 1 fs. To determine the melting temperature, the technique proposed by Morris *et al.*[66] was used. This process involved allowing one slab of zb CdTe crystal and one slab of liquid CdTe to be in contact and reach an equilibrium temperature. We began with a single crystalline zb CdTe crystal containing 7200 atoms constructed using the 0 K lattice parameter. The simulations employed periodic boundary conditions in all three coordinate directions. The crystalline half of the block contained 3600 atoms whose positions were held fixed while the temperature of the other 3600 atoms was increased to 2700 K over a 0.1 ns period. The pressure was held at 1 atm while maintaining the desired temperature under NPT (constant mass, pressure, and temperature) conditions using a Nosè-Hoover thermostat/barostat[65,67] with a temperature damping parameter of 10.0, a pressure damping parameter of 5.0, and a drag coefficient of 1.0. The constant pressure condition ensured that the sample dimension could relax, thereby removing any unrealistic stresses in the melt. After reaching a constant temperature for 0.05 ns, the fixed crystal was released. Isenthalpic (NPH) dynamics were then performed for

TABLE VII. Melting temperatures of zinc-blende CdTe(K).

Expt.	1365
SW	1360–1390
TR	700–800

0.2 ns to bring the two slabs into thermal equilibrium where the system temperature was well converged. Another 0.05 ns simulation was conducted, and the melting temperature was calculated as the average temperature in the final 0.05 ns period. The results obtained are shown in Table VII. The SW potential has a melting temperature of 1360–1390 K, very close to the experimental value of 1365 K,[68] but the TR potential has a much lower melting temperature of 700–800 K. The low melting temperature of the TR potential is consistent with the cohesive energy data shown in Fig. 1 which shows that the zb CdTe is not even stable compared to CsCl and NaCl structures.

VII. VAPOR DEPOSITION SIMULATIONS

Simulating vapor deposition is another excellent test of a potential. Beginning with a substrate of zb CdTe and randomly dropping atoms onto the surface at elevated temperatures, a vapor deposition process would sample many local configurations that can possibly form on the surface but cannot be included in similar studies described in the previous sections. If a potential truly has the lowest energy for the equilibrium zb CdTe and proper energy trend driving the evolution of metastable configurations towards the equilibrium structure, a crystalline growth of the lowest energy phase is likely to be obtained in the simulations. On the other hand, if a surface asperity has an incorrect low energy, it is likely to be retained and trigger the growth of an amorphous structure.

To model the deposition we began with a 3.2×3.2 nm^2 substrate with a thickness of 1.4 nm consisting of 1000 atoms. The bottom 2 atomic layers of the substrate were held fixed, 3 layers of atoms above the fixed region were isothermally controlled, and 3 layers of atoms at the surface were left free. NVT dynamics were used to maintain the isothermal temperature at 1000 K for SW and 400 K for TR. TR requires a lower temperature because of the much lower melting temperature for the potential. Adatoms with an initial incident energy of 0.5 eV and an initial incident direction perpendicular to the growth surface were placed at random locations far above the substrate. The atom types were chosen such that over time the composition would be statistically stoichiometric. An adatom injection frequency corresponding to a growth rate of 0.5 nm/ns was used. The time step of the MD simulations was 1 fs.

Figures 6(a) and 6(b) show, respectively, the SW and TR simulated structures of the films after 3.3 ns of deposition. The SW potential did simulate crystalline growth of the zb structure. In contrast, the TR potential produced an amorphous structure. Performing deposition simulations at other temperatures using the TR potential also resulted in the amorphous growth. Figure 6(b) also indicates that not only the deposited atoms formed the amorphous structure, but also the non-fixed atoms in the initial zb structure transformed to the amorphous structure. These findings are all consistent with Fig. 1 that the TR potential does not give zb CdTe structure as the lowest energy phase.

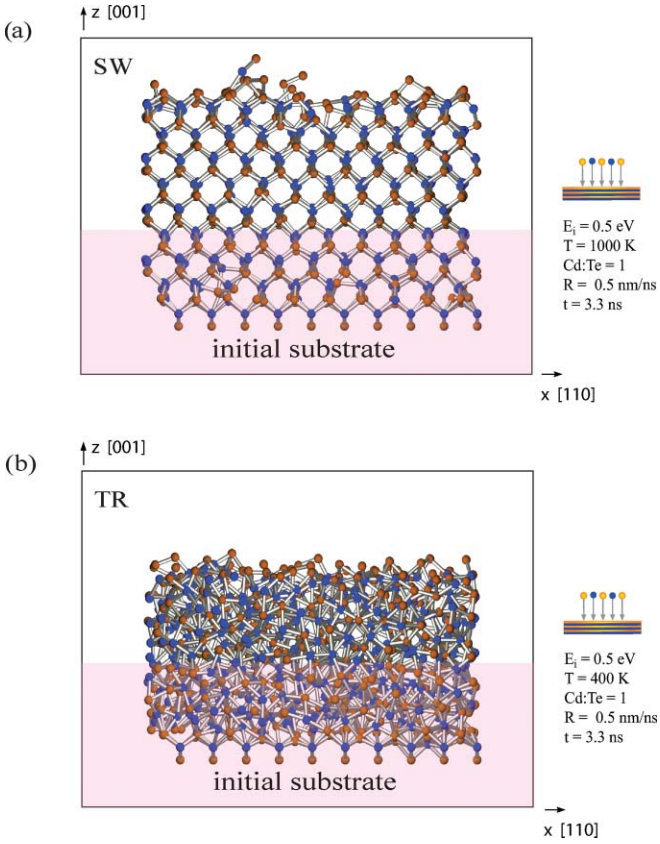

FIG. 6. Thin film structures after 3.3 ns deposition obtained from (a) SW potential at 1000 K and (b) TR potential at 400 K. The light atoms (orange) are Cd and the dark atoms (blue) are Te.

VIII. TOWARDS MORE ACCURATE MODELS

The above analysis indicates that for the CdTe interatomic potentials currently available in the literature, the SW parameterization has clear advantages over the TR parameterization. Most importantly, the SW parameterization has the correct lowest energy, melting temperature and crystalline growth of the ground state zb CdTe structure, none of which could be captured by the TR parameterization. This means that the SW parameterization can be used to simulate CdTe for some specific properties. However, neither SW nor TR parameterizations result in a correct trend for energies and dimensions of a variety of configurations. In particular, both result in incorrect lowest energy elemental structures. Additionally, they are not accurate in predicting defect and surface energies. Numerous methods can be implemented to develop a more transferrable potential for MD simulations of defect interaction and formation under thermomechanical conditions. These are described here.

As described in Appendix A, not all the parameters in the SW parameterization were optimized. At first sight, it appears that the SW potential can be significantly improved if all the

parameters are optimized. However, it should be noted that the SW potential is empirically constructed for the dc or zb structures. This can be seen from Eq. (A1), where the angular term is essentially a parabolic energy penalty for any structures with bond angles deviating from the tetrahedral angles of dc and zb structures. While this facilitates a lowest energy dc or zb phase, it does not physically ensure the distribution of bond length and energies of other phases. We can examine this in more detail.

Consider a diamond-cubic or zinc-blend structure under hydrostatic strain, the bond angles remain constant at the tetrahedral angle and the angular term of Eq. (A1) diminishes. This means that the SW potential reduces to a pair potential model for a ground state diamond-cubic or zinc-blend structure under hydrostatic strain. Equation (A2) indicates that the pair component of the SW potential essentially has four parameters $p_1 = e_{ij}A_{ij}$, $p_2 = B_{ij}$, $p_3 = \sigma_{ij}$, and $p_4 = a_{ij}\sigma_{ij}$. However, only three of these four parameters are independent due to the constraint on the relative hardness of the repulsive interaction with that of the attractive interaction. This can be seen more clearly using the general Lennard-Jones (LJ) and Morse pair potentials which also have four parameters A, B, α, and β. It is well known that two of the four parameters α and β satisfy the relation $\alpha/\beta \sim 2$ for most materials (e.g., 6–12 LJ) in order to give a reasonable relative hardness. In general, the four parameters of the pair component of the SW potential can be fully determined by four properties of a dc or a zb structure: lattice constant, cohesive energy, bulk modulus, and relative hardness. Under that condition, the angular term is required to fit many properties including other shear moduli and melting temperature of the dc or zb structure, and energies and dimensions of other lattices, defects, and surface configurations, which is in general difficult. Note that the SW potential does not have to be used for tetrahedral structures. For non-tetrahedral structures, the angular term does not diminish and the simple function form is no longer an advantage of the SW potential as compared to the Tersoff potential.

While the SW potential is not fundamentally transferrable, it can be easily parameterized to ensure the tetrahedral structure to have the lowest energy and the crystalline growth of the tetrahedral structure during vapor deposition simulations. It can be seen from Eqs. (A1) and (A3) that the angular penalty term essentially scales with the parameter λ_{ij} (assume $\lambda_{ij} = \lambda_{ik} = \lambda$). As a result, SW potential always ensures the lowest energy and the crystalline growth of the tetrahedral structure when λ is above a critical value. Likewise, the SW potential may fail to reproduce the lowest energy and crystalline growth of the tetrahedral structure when λ is small. To test how sensitively the SW potential depends on λ, we performed MD simulations of vapor deposition of CdTe using a slightly reduced λ value of 21 (original value 25) and a much larger value of 50. The results are shown, respectively, in Figs. 7(a) and 7(b). Clearly, the deposited film degraded to an amorphous structure even when λ is slightly reduced, but continues to produce crystalline growth when doubled. Due to the restriction of λ being constrained above a critical level, it is more difficult for the SW potential to fit the property trend for many stable and unstable configurations.

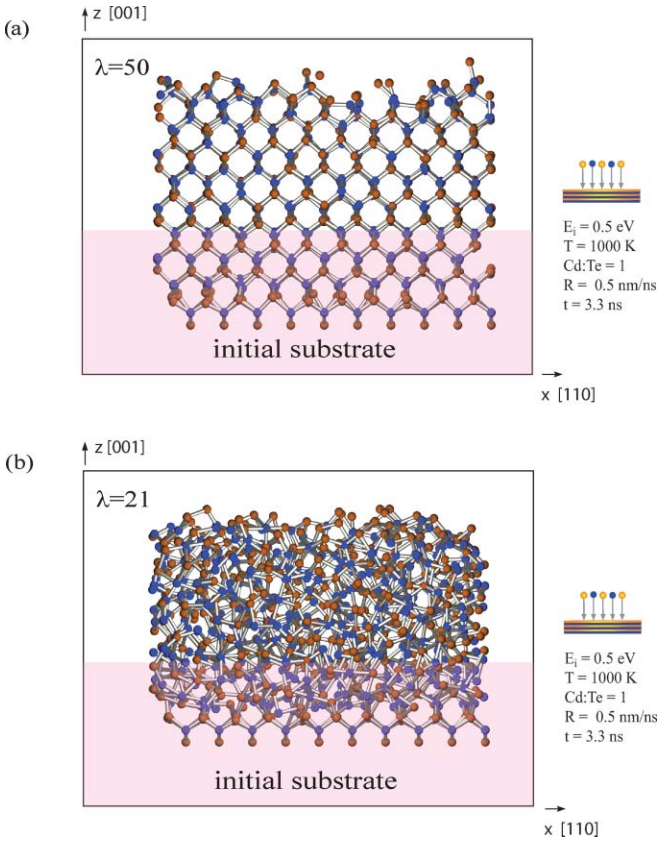

FIG. 7. Thin film structures after 3.3 ns deposition obtained from SW potential at 1000 K with (a) $\lambda = 50$ and (b) $\lambda = 21$. The light atoms (orange) are Cd and the dark atoms (blue) are Te.

While our studies showed some problems of the TR CdTe potential, this is likely due to the parameterization rather than the potential format considering that Tersoff[46] and Brenner[69] types of potentials have been very successfully applied for carbon nanotubes,[70] SiC,[71–73] GaAs,[85] and GaN.[86] In the Tersoff energy expression equation (A4), the first term is a sum of pairwise energies representing the core-core repulsion between atoms. This is different from the SW potential where the pairwise sum represents total interaction including both repulsion and attraction. The second term in Eq. (A4) is a sum of the product between the bond order and pairwise bond integral representing the bonding energy between atoms. Bond order is defined as one-half the difference of the number of bonding and antibonding electrons in the molecular orbitals between adjacent atoms,[74] and the bond integral is related to the probability that an electron hops from one molecular orbital to another. Such a potential format can be strictly derived from quantum mechanical theories[75–83] and hence the Tersoff potential can be highly transferrable if well parameterized. Unfortunately, there is no obvious approach to ensure the lowest energy for the tetrahedral structure with the Tersoff potential. To ensure a correct simulation of a tetrahedral structure and its crystalline growth, energies of a large number of clusters, lattices, defects, and surfaces need to be specifically fitted. Since the energy of the tetrahedral structure must be lower than any other structure, it is also not clear which configurations need to be included in the fitting. As a result, it is

not surprising that parameterizations of the Tersoff potential might result in amorphous film growth, as seen here. Nonetheless, well parameterized Tersoff potentials have been developed for a number of systems,[84,85] and have simulated crystalline growth for GaN and GaAs.[86,87] The Tersoff-Rockett potential explored here only fit the Cd-Te parameters while the Cd-Cd and Te-Te parameters were simply taken to be the literature values of Si (See Appendix A). The TR potential can be significantly improved if all the parameters are optimized.

To explore how the TR model can be improved in detail, we consider structures with only the nearest neighbor interactions. For such structures, all bonds are equivalent. From Eq. (A4), we can write the bond energy E_b as a function of bond length r as

$$E_b = \phi(r) + \Theta \cdot u(r). \tag{4}$$

Note that for simplicity, we have combined the pair function here so that $f_c(r) \cdot \phi(r) \Rightarrow \phi(r)$ and $f_c(r) \cdot u(r) \Rightarrow u(r)$. When the structures are subject to hydrostatic strain, bond angles remain constant. Equations (A5) and (A9)–(A11) indicate that the bond order Θ would be a constant for a bond length range $r \leq R_c - D_c$. At the equilibrium bond length, $\partial E_b/\partial r = 0$, and Eq. (4) then gives

$$\Theta = -\frac{\phi'(r)}{u'(r)}. \tag{5}$$

Substituting Eq. (5) into Eq. (4), we have an expression for equilibrium bond energy $E_{b,0}$ as a function of equilibrium bond length r_0:

$$E_{b,0} = \phi(r_0) - \frac{\phi'(r_0)}{u'(r_0)} \cdot u(r_0). \tag{6}$$

Likewise, we can write the second derivative of the bond energy with respect to bond length using the equilibrium condition:

$$E''_{b,0} = \phi''(r_0) - \frac{\phi'(r_0)}{u'(r_0)} \cdot u''(r_0). \tag{7}$$

Equations (6) and (7) are necessary conditions that any nearest neighbor structure must satisfy. In practice, if the target values of cohesive energies, lattice constants, and bulk moduli of a variety of nearest neighbor structures (e.g., dimer, dc, sc, fcc, hcp, NaCl, zb, etc.) are known from either experiments or *ab initio* calculations, then these cohesive energies, lattice constants, and bulk moduli can be converted to bond energies, bond lengths, and second derivatives of bond energy, respectively. The converted data points can then be fitted to Eqs. (6) and (7). The ability to fit the lattice constants, cohesive energies, and bulk moduli for a variety of phases with two x-y curves accounts for the transferability of the Tersoff potential. Equations (6) and (7) suggest a two-step parameterization approach that can overcome the difficulties in parameterizing a transferrable Tersoff potential. First, the pair potential parameters can be fully determined by fitting the energies, lattice constants, and bulk moduli of a variety of nearest neighbor phases using Eqs. (6) and (7). The second step involves determining the bond order parameters by fitting the bond orders of nearest neighbor structures to Eq. (5) and other properties, including those of other (non-nearest neighbor) structures. Such a strategy has been successfully applied in parameterizing GaN and GaAs potentials.[84–87]

Tersoff type of potentials can be viewed as the simplest bond order potential (BOP) (Ref. 75) which incorporates only the two-hop effect of electrons. It does neither distinguish between σ and π bonding nor address the valence effects. More accurate bond order potentials have been analytically derived[75–83] from quantum mechanical theories under the condition that the first two levels of the expanded Greens function for the σ and π bond orders are retained. The full BOP formalism includes separate contributions from molecular orbitals describing σ and π type bonds[80] and can be applied not only to open phase (half-full valence shell) materials but also to close-packed structures,[81] and compounds.[75] Recently, the BOP approach has been generalized to more effectively model sp-valent elements in material systems where the degree of valence shell filling is incorporated.[83] The complete BOP incorporates 4-hop effects of electrons. While the complete BOP can be in principle much more transferrable than the Tersoff and Brenner types of potentials, its parameterization is also much more challenging. In a previous effort, Murdick *et al*. successfully parameterized an analytical BOP for GaAs and demonstrated its transferability to a variety of phases and defect configurations.[47] This GaAs BOP has also been successfully applied in vapor deposition simulations of zb GaAs and the many condensation mechanisms revealed in the simulations are in good agreement with experiments.[88] Currently, we have also developed a complete analytical BOP for CdTe capable of Cd, Te, and CdTe crystalline growth.[89] Although details about this potential will be given in a separate paper, Fig. 8 shows an example of the CdTe growth simulation using the new BOP. Similar to the SW potential examined here, the BOP correctly captures the crystalline growth during vapor deposition of the zb CdTe, but is not limited

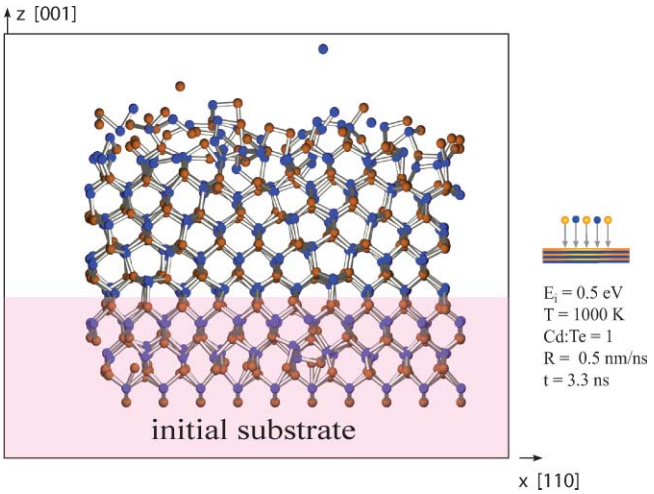

FIG. 8. Thin film structures after 3.3 ns deposition obtained from bond order potential at 1000 K. The light atoms (orange) are Cd and the dark atoms (blue) are Te.

by the structure restrictions associated with the SW potential. Note that this BOP also has the correct lowest energy Cd, Te, and CdTe phases.

IX. CONCLUSIONS

A thorough study has been conducted to evaluate the CdTe interatomic potentials currently available in literature. First, the structures and energies of a variety of elemental and compound lattices, defects, and surfaces were calculated and compared to those obtained from our *ab initio* calculations and literature experimental results. This is complemented by melting temperature calculations and vapor deposition simulations. The following conclusions have been reached:

1. The existing Stillinger-Weber and Tersoff-Rockett parameterizations of the CdTe potential both have incorrect lowest energy elemental Cd and Te structures. Hence, they cannot be used for Cd or Te simulations. In addition, both parameterizations do not capture the lowest energy surface reconstructions of the zinc-blende CdTe compound.
2. The Stillinger-Weber parameterization of the CdTe potential correctly reproduces the melting temperature, the lowest energy, and the crystalline growth for the ground state zinc-blende structure of CdTe, and hence can be used to study CdTe for specific properties. Contrarily, the Tersoff-Rockett parameterization of the CdTe potential predicts a wrong melting temperature and an amorphous growth of the zinc-blende CdTe, and a wrong B2 (CsCl) structure for CdTe. The Tersoff-Rockett parameterization, therefore, cannot be used for CdTe simulations.
3. Due to its incorrect elemental structures and energies, the Stillinger-Weber parameterization cannot correctly capture heat of mixing and defect formation energies (with respect to elemental phases) for the CdTe compound. Hence, the potential should not be used to study structure evolution, defect formation, and defect interaction processes even for zinc-blende CdTe.
4. The Stillinger-Weber parameterization has reasonable elastic properties for open structures like zinc-blende CdTe, but significantly over predicts the elastic constants for closely packed structures. Consequently, simulations to study mechanical properties during high pressure and high density should be avoided with the Stillinger-Weber parameterization.
5. While the Stillinger-Weber parameterization can be improved by optimizing all parameters, the transferability of the potential is limited by the fundamental flaw of the potential format. While we showed that the Tersoff-Rockett parameterization is inferior to the Stillinger-Weber parameterization, this is due to the parameterization rather than the potential format. We demonstrated that a two-step parameterization can improve the transferability of the Tersoff-Rockett potential beyond that of the Stillinger-Weber potential. Further, full bond-order potentials are capable of resolving many of the issues associated with SW and TR potentials as demonstrated by the vapor deposition example.

ACKNOWLEDGMENTS

This work is supported by the NNSA/DOE Office of Nonproliferation Research and Development, Proliferation Detection Program, Advanced Materials Portfolio. Sandia National Laboratories is a multi-program laboratory managed and operated by Sandia Corporation, for the U.S. Department of Energy's National Nuclear Security Administration under Contract No. DE-AC04-94AL85000.

APPENDIX A: APPROXIMATIONS OF POTENTIAL PARAMETERS

The two potentials examined here are the Stillinger-Webber (SW) potential parameterized by Wang *et al.*[40] and the Tersoff-Rockett (TR) potential parameterized by Oh and Grein.[36] Both potentials involve some simplifications in their parameterizations. These simplifications may explain some of our results and are therefore discussed here.

The SW potential can be rewritten as

$$E = \frac{1}{2}\sum_i \sum_{j\neq i} \phi_{ij}(r_{ij}) + \frac{1}{2}\sum_i \sum_{j\neq i} \sum_{k\neq j\neq i} u_{ij}(r_{ij}) \cdot u_{ik}(r_{ik}) \cdot \left[\cos\left(\theta_{jik}\right) + \frac{1}{3}\right]^2, \tag{A1}$$

where $\phi_{ij}(r_{ij})$ and $u_{ij}(r_{ij})$ are pairwise functions of atomic spacing r with subscripts indicating either species or identification of atoms, and θ_{jik} represents the bond angle at atom i formed by the bond vectors from atom i to neighboring atoms j and k. The pair functions $\phi_{ij}(r_{ij})$ and $u_{ij}(r_{ij})$ are written respectively as

$$\phi_{ij}(r_{ij}) = \begin{cases} \varepsilon_{ij} A_{ij} \left(\frac{B_{ij}}{r^4} - 1\right) \exp\left(\frac{\sigma_{ij}}{r_{ij} - a_{ij}\sigma_{ij}}\right) & , r_{ij} \leq a_{ij}\sigma_{ij} \\ 0 & , r_{ij} > a_{ij}\sigma_{ij} \end{cases}, \tag{A2}$$

$$u_{ij}(r_{ij}) = \begin{cases} \sqrt{\varepsilon_{ij}\lambda_{ij}} \exp\left(\frac{\gamma_{ij}\sigma_{ij}}{r_{ij} - a_{ij}\sigma_{ij}}\right), & r_{ij} \leq a_{ij}\sigma_{ij} \\ 0 & , \quad r_{ij} > a_{ij}\sigma_{ij} \end{cases}. \tag{A3}$$

Here, ε_{ij}, λ_{ij}, γ_{ij}, A_{ij}, B_{ij}, σ_{ij}, and a_{ij} are pairwise parameters, and in particular, $a_{ij}\sigma_{ij}$ is the pairwise cutoff distance of the potential. For the CdTe system, the seven parameters ε_{ij}, λ_{ij}, γ_{ij}, A_{ij}, B_{ij}, σ_{ij}, and a_{ij} in Eqs. (A1)–(A3) must be defined for each of the three pairs ij = CdCd, TeTe, and CdTe. Not all these parameters were optimized in Wang *et al.*'s parameterization.[40] For example, the parameters ε_{ij}, λ_{ij}, γ_{ij}, σ_{ij}, and a_{ij} were chosen to be the same for all (CdCd, TeTe, CdTe) pairs, and in particular γ_{ij} and a_{ij} were simply taken as the literature values for Si.[44] This leaves A_{ij} and B_{ij} as the only parameters to be optimized. It is thus not

surprising that Wang *et al.*'s parameterization[40] did not best capture the elemental energy trends, defect energies, and many of the elastic properties for high density structures.

The Tersoff-Rockett potential[45] can be rewritten as

$$E = \frac{1}{2}\sum_i \sum_{j\neq i} [f_{c,ij}(r_{ij}) \cdot \phi_{ij}(r_{ij}) + \Theta_{ij} \cdot f_{c,ij}(r_{ij}) \cdot u_{ij}(r_{ij})], \tag{A4}$$

where $\phi_{ij}(r_{ij})$ and $u_{ij}(r_{ij})$ are pairwise repulsive and attractive potential functions in the original Tersoff potential,[46] $f_{c,ij}(r_{ij})$ is a cutoff function, and Θ_{ij} is the bond order for the ij bond. The cutoff function is defined as

$$f_{c,ij}(r_{ij}) = \begin{cases} 1, & r_{ij} \leq R_{c,ij} - D_{c,ij} \\ \frac{1}{2} - \frac{1}{2}\cos\left(\frac{\pi}{2}\frac{r_{ij}-R_{c,ij}}{D_{c,ij}}\right), & R_{c,ij} - D_{c,ij} < r \leq R_{c,ij} + D_{c,ij}, \\ 0, & r > R_{c,ij} + D_{c,ij} \end{cases} \tag{A5}$$

where $R_{c,ij}$ and $D_{c,ij}$ are pairwise parameters and in particular, $R_{c,ij} + D_{c,ij}$ is the cutoff distance of the ij pair functions. The pair functions $\phi_{ij}(r_{ij})$ and $u_{ij}(r_{ij})$ are defined respectively as

$$\phi_{ij}(r_{ij}) = \begin{cases} A_{ij}\exp(-\alpha_{ij} r_{ij}), & r_{ij} \leq R_{a,ij} - D_{a,ij} \\ f_{a,ij}(r_{ij}) A_{ij}\exp(-\alpha_{ij} r_{ij}), & R_{a,ij} - D_{a,ij} < r_{ij} \leq R_{a,ij} + D_{a,ij} \\ 0, & r_{ij} > R_{a,ij} + D_{a,ij} \end{cases}, \tag{A6}$$

$$u_{ij}(r_{ij}) = \begin{cases} -B_{ij}\exp(-\beta_{ij} r_{ij}), & r_{ij} \leq R_{a,ij} - D_{a,ij} \\ -B_{ij}\exp(-\beta_{ij} r_{ij}) - [f_{a,ij}(r_{ij}) - 1] A_{ij}\exp(-\alpha_{ij} r_{ij}), & R_{a,ij} - D_{a,ij} < r_{ij} \leq R_{a,ij} + D_{a,ij} \\ -B_{ij}\exp(-\beta_{ij} r_{ij}) + A_{ij}\exp(-\alpha_{ij} r_{ij}), & r_{ij} > R_{a,ij} + D_{a,ij} \end{cases}, \tag{A7}$$

where A_{ij}, B_{ij}, α_{ij}, β_{ij}, $R_{a,ij}$, and $D_{a,ij}$ are all pairwise parameters, and $f_{a,ij}(r_{ij})$ is another cutoff function similar to Eq. (A5) but with a shorter cutoff distance $R_{a,ij} + D_{a,ij}$:

$$f_{a,ij}(r_{ij}) = \begin{cases} 1, & r_{ij} \leq R_{a,ij} - D_{a,ij} \\ \frac{1}{2} - \frac{1}{2}\cos\left(\frac{\pi}{2}\frac{r_{ij}-R_{a,ij}}{D_{a,ij}}\right), & R_{a,ij} - D_{a,ij} < r_{ij} \leq R_{a,ij} + D_{a,ij} \\ 0, & r_{ij} > R_{a,ij} + D_{a,ij} \end{cases}. \tag{A8}$$

It can be seen from the third splined function in Eqs. (A6) and (A7) that the "repulsive" term $\phi_{ij}(r_{ij})$ decays to zero and the bond order modified "attractive" term $u_{ij}(r_{ij})$ evolves to a full interaction potential (i.e., including both repulsion and interaction) over the atomic spacing range between $R_{a,ij} - D_{a,ij}$ and $R_{a,ij} + D_{a,ij}$. This is different from the original Tersoff potential where $\phi_{ij}(r_{ij})$ always represents a positive repulsive energy, $u_{ij}(r_{ij})$ always represents an attractive function, and the bond order always modifies only the attractive function.

The bond order is calculated as

$$\Theta_{ij} = (1 + \eta_{ij}^{n_{ij}} \zeta_{ij}^{n_{ij}})^{-\frac{1}{2n_{ij}}}, \tag{A9}$$

where n_{ij} and η_{ij} are pairwise parameters and the local variable ζ_{ij} is expressed as

$$\zeta_{ij} = \sum_{k\neq i\neq j} f_{c,ik}(r_{ik}) g_{ik}(\theta_{jik}) \exp[\lambda_{ik}^{m_{ik}}(r_{ij} - r_{ik})^{m_{ik}}], \tag{A10}$$

where λ_{ik} and m_{ik} are pairwise parameters, and the angular function $g_{ik}(\theta_{jik})$ is written as

$$g_{ik}(\theta_{jik}) = \gamma_{ik}\left[1 + \frac{c_{ik}^2}{d_{ik}^2} - \frac{c_{ik}^2}{d^2 + (h_{ik} - \cos\theta_{jik})^2}\right]. \tag{A11}$$

Here, γ_{ik}, c_{ik}, d_{ik}, and h_{ik} are four additional pairwise parameters.

The Tersoff-Rockett CdTe potential has 16 parameters A_{ij}, B_{ij}, α_{ij}, β_{ij}, n_{ij} η_{ij}, λ_{ik}, m_{ik}, γ_{ik}, c_{ik}, d_{ik}, h_{ik}, $R_{a,ij}$, $D_{a,ij}$, $R_{c,ij}$, and $D_{c,ij}$ for each of the three pairs CdCd, TeTe, and CdTe. In the parameterization by Oh and Grein,[36] not all these parameters are optimized for CdTe. In particular, the parameters n_{ij}, η_{ij}, λ_{ik}, m_{ik}, γ_{ik}, c_{ik}, d_{ik}, h_{ik} are all taken from the literature values of Si.[46] This lack of careful parameterization accounts for our observation that Oh and Grein's parameterization[36] cannot capture the melting temperature or crystalline growth of CdTe zb or any significant properties of the elemental phases.

APPENDIX B: DENSITY FUNCTIONAL THEORY CALCULATIONS

We performed electronic structure calculations within the generalized gradient approximation (GGA) using projector augmented wave (PAW) pseudopotentials as implemented in the Vienna *Ab initio* Simulation Package (VASP).[90] All calculations utilized the non-empirical PBE GGA functional[91] and were carried out with unconstrained, spin-polarized conditions. This is necessary for calculating CdTe cohesive energies since the ground state of the Te atom is an electronic triplet state. For the cohesive energy calculations, the cutoff energy for the plane wave basis set was set to 500 eV, and the Brillouin zone was sampled using a dense $10 \times 10 \times 10$ Gamma-centered Monkhorst-Pack grid. Defect energy calculations required the use of very large $3 \times 3 \times 3$ supercells (> 200 atoms) and, therefore, a smaller 300 eV cutoff energy and a $2 \times 2 \times 2$ Gamma-centered Monkhorst-Pack grid was utilized. In our DFT calculations, both the atomic positions and cell parameters in all the systems were fully relaxed.

[1] L. L. Kazmerski, J. Electron Spectrosc. Relat. Phenom. **150**, 105 (2006).
[2] J. J. Loferski, J. Appl. Phys. **27**, 777 (1956).
[3] G. S. Khrypunov, E. P. Chernykh, N. A. Kovtun, and E. K. Belonogov, Semiconductors **43**, 1046 (2009).
[4] R. H. Bube and K. W. Mitchell, J. Electron. Mater. **22**, 17 (1993).
[5] H. C. Chou and A. Rohatgi, J. Electron. Mater. **23**, 31 (1994).
[6] W. H. Bloss, F. Pfisterer, M. Schubert, and T. Walter, Prog. Photovoltaics **3**, 3 (1995).
[7] M. D. G. Potter, M. Cousins, K. Durose, and D. P. Halliday, J. Mater. Sci.: Mater. Electron. **11**, 525 (2000).
[8] T. E. Schlesinger, J. E. Toney, H. Yoon, E. Y. Lee, B. A. Brunett, L. Franks, and R. B. James, Mater. Sci. Eng. R. **32**, 103 (2001).
[9] P. J. Sellin, Nucl. Instrum. Methods Phys. Res. A **513**, 332 (2003).
[10] A. Peurrung, Mater. Today **11**, 50 (2008).
[11] T. Takahashi and S. Watanabe, IEEE Trans. Nucl. Sci. **48**, 950 (2001).
[12] C. Scheiber, Nucl. Instrum. Methods Phys. Res. A **380**, 385 (1996).
[13] L. Verger, J. P. Bonnefoy, F. Glasser, and P. Ouvrier-Buffet, J. Electron. Mater. **26**, 738 (1997).
[14] C. Szeles, Phys. Status Solidi B **241**, 783 (2004).
[15] A. Shah, P. Torres, R. Tscharner, N. Wyrsch, and H. Keppner, Science **285**, 692 (1999).
[16] J. D. Beach and B. E. McCandless, MRS Bull. **32**, 225 (2007).
[17] K. D. Dobson, I. Visoly-Fisher, G. Hodes, and D. Cahen, Sol. Enery Mater. Sol. Cells **62**, 295 (2000).
[18] A. Rohatgi, R. Sudharsanan, S. A. Ringel, and M. H. MacDougal, Sol. Cells. **30**, 109 (1991).
[19] J. Versluys, P. Clauws, P. Nollet, S. Degrave, and M. Burgelman, Thin Solid Films **451–452**, 434 (2004).
[20] Y. Yan, M. M. Al-Jassim, and K. M. Jones, J. Appl. Phys. **94**, 2976 (2003).
[21] J. R. Heffelfinger, D. L. Medlin, and R. B. James, in *Proceedings of the SPIE Conference on HardX-Ray and Gamma-Ray Detector Physics and Applications*, edited by F. P. Doty and R. B. Hoover (SPIE, Bellingham, WA, 1998), Vol. 3446, p. 49.
[22] J. R. Heffelfinger, D. L. Medlin, and R. B. James, *Proceedings of the Materials Research Society Symposium on Semiconductors for Room-Temperature Radiation Detector Applications II*, edited by R. B. James (MRS Warrendale, PA, 1998), Vol. 487, p. 33.
[23] J. R. Heffelfinger, D. L. Medlin, H. Yoon, H. Hermon, and R. B. James, in *Proceedings of the SPIE Conference on Hard X-ray and Gamma-ray Detector Physics, Optics and Application*, edited by R. B. Hoover and F. P. Doty (SPIE, Bellingham, WA, 1997), Vol. 3115, p. 40.
[24] A. E. Bolotnikov, G. S. Camarda, G. A. Carini, Y. Cui, L. Li, and R. B. James, Nucl. Instrum. Methods Phys. Res. A **579**, 125 (2007).
[25] A. E. Bolotnikov, G. S. Camarda, G. A. Carini, Y. Cui, L. Li, and R. B. James, Nucl. Instrum. Methods Phys. Res. A **571**, 687 (2007).
[26] G. Zha, W. Jie, T. Tan, and L. Wang, Phys. Status Solidi A **204**, 2196 (2007).
[27] S. H. Shin, J. Bajaj, L. A. Moudy, and D. T. Cheung, App. Phys. Lett. **43**, 68 (1983).
[28] K. Yokota, T. Yoshikawa, S. Katayama, S. Ishihara, and I. Kimura, Jap. J. App. Phys. **24**, 1672 (1985).
[29] R. S. Rai, S. Mahajan, S. McDefitt, and C. J. Johnson, J. Vac. Sci. Technol. B **9**, 1892 (1991).
[30] R. D. S. Yadava, R. K. Bagai, and W. N. Borle, J. Electron. Mater. **21**, 1001 (1992).
[31] P. Rudolph, M. Neubert, and M. Mühlberg, J. Crys. Growth **128**, 582 (1993).
[32] L. Turjanska, P. Höschl, E. Belas, R. Grill, J. Franc, and P. Moravec, Nucl. Instrum. Methods Phys. Res. A **458**, 90 (2001).
[33] S.-H. Wei and S. B. Zhang, Phys. Rev. B **66**, 155211 (2002).
[34] G. A. Carini, A. E. Bolotnikov, G. S. Camarda, G. W. Wright, R. B. James, and L. Li, App. Phys. Lett. **88**, 143515 (2006).
[35] P. Rudolph, Cryst. Res. Technol. **38**, 542 (2003).
[36] J. Oh and C. H. Grein, J. Cryst. Growth **193**, 241 (1998).
[37] M. B. Kanoun, W. Sekkal, H. Aourag, and G. Merad, Phys. Lett. A **272**, 113 (2000).
[38] J. P. Rino, P. S. Branício, and D. S. Borges, Defect Diffus. Forum **258–260**, 522 (2006).
[39] Z. Q. Wang and D. Stroud, Phys. Rev. B **38**, 1384 (1988).
[40] Z. Q. Wang, D. Stroud, and A. J. Markworth, Phys. Rev. B **40**, 3129 (1989).
[41] B. K. Agrawal and S. Agrawal, Phys Rev. B **45**, 8321 (1992).
[42] M.-H. Du, H. Takenaka, and D. J. Singh, Phys Rev. B **77**, 094122 (2008).
[43] S. Gundel, A. Fleszar, W. Faschinger, and W. Hanke, Phys. Rev. B **59**, 15261 (1999).
[44] F. H. Stillinger and T. A. Weber, Phys. Rev. B **31**, 5262 (1985).
[45] J. Wang and A. Rockett, Phys. Rev. B **43**, 12571 (1991).
[46] J. Tersoff, Phys. Rev. B **39**, 5566 (1989).
[47] D. A. Murdick, X. W. Zhou, H. N. G. Wadley, D. Nguyen-Manh, R. Drautz, and D. G. Pettifor, Phys. Rev. B **73**, 45206 (2006).
[48] J. D. H. Donnay and H. M. Ondik, *Crystal Data, Determinative Tables*, Inorganic Compounds Vol. 2, 3rd ed. (U. S. Department of Commerce, National Bureau of Standards, and Joint Committee on Power Diffraction Standards, U.S.A., 1973).
[49] I. Barin, *Thermochemical Data of Pure Substances*, (VCH, Weinheim, 1993).
[50] S. Plimpton, J. Comp. Phys **117**, 1 (1995).
[51] M. Parrinello and A. Rahman, J. Appl. Phys. **52**, 7182 (1981).
[52] B. M. Wong, J. Comput. Chem. **30**, 51 (2009).
[53] B. M. Wong, D. Lacina, I. M. B. Nielsen, J. Graetz, and M. D. Allendorf, J. Phys. Chem. C **115**, 778 (2011).
[54] I. Barin, *Thermochemical Data of Pure Substances* (VCH, Weinheim, 1993).
[55] E. R. Cowley, Phys. Rev. Lett. **60**, 2379 (1988).
[56] X. W. Zhou and R. E. Jones, Modell. Simul. Mater. Sci. Eng. **19**, 25004 (2011).
[57] C. Szeles, IEEE Trans. Nucl. Sci. **51**, 1242 (2004).
[58] S. B. Zhang and J. E. Northrup, Phys. Rev. Lett. **67**, 2339 (1991).
[59] J. E. Northrup and S. B. Zhang, Phys. Rev. B **47**, 6791 (1993).
[60] L. Seehofer, G. Falkenberg, R. L. Johnson, V. H. Etgens, S. Tatarenko, D. Brun, and B. Daudin, Appl. Phys. Lett. **67**, 1680 (1995).
[61] B. Daudin, D. Brun-Le Cunff, and S. Tatarenko, Surf. Sci. **352–354**, 99 (1996).
[62] M. B. Veron, V. H. Etgens, M. Sauvage-Simkin, S. Tatarenko, B. Daudin, and D. Brun-Le Cunff, J. Cryst. Growth **159**, 694 (1996).
[63] S. Tatarenko, B. Daudin, D. Brun, V. H. Etgens, and M. B. Veron, Phys. Rev. B **50**, 18479 (1994).
[64] G.-X. Qian, R. M. Martin, and D. J. Chadi, Phys. Rev. B **38**, 7649 (1988).
[65] M. E. Tuckerman, J. Alejandre, R. López-Rendón, A. L. Jochim, and G. J. Martyna, J. Phys. A **39**, 5629 (2006).
[66] J. R. Morris, C. Z. Wang, K. M. Ho, and C. T. Chan, Phys. Rev. B **49**, 3109 (1994).
[67] W. Shinoda, M. Shiga, and M. Mikami, Phys. Rev. B **69**, 134103 (2004).
[68] I. S. Grigoriev and E. Z. Meilikhov, *Handbook of Physical Quantities* (CRC Press, New York, 1997).
[69] D. W. Brenner, Phys. Rev. B **42**, 9458 (1990).
[70] E. H. Feng and R. E. Jones, Phys. Rev. B **81**, 125436 (2010).
[71] H. Yan, X. Hu, and H. Jónsson, Surf. Sci. **316**, 181 (1994).
[72] A. J. Dyson and P. V. Smith, Surf. Sci. **396**, 24 (1998).
[73] F. Gao and W. J. Weber, Nucl. Instrum. Methods Phys. Res. B **191**, 504 (2002).
[74] D. G. Pettifor, *Bonding and Structure of Molecules and Solids* (Oxford University Press, Oxford, 1995).

[75]D. G. Pettifor, M. W. Finnis, D. Nguyen-Manh, D. A. Murdick, X. W. Zhou, and H. N. G. Wadley, Mater. Sci. Eng. A **365**, 2 (2004).
[76]M. Finnis, *Interatomic Forces in Condensed Matter Oxford Series on Materials Modelling* (Oxford University Press, Oxford, 2003).
[77]D. G. Pettifor, Phys. Rev. Lett. **63**, 2480 (1989).
[78]D. G. Pettifor, in *Many Atom Interactions in Solids*, edited by R. M. Nieminen, M. J. Puska, and M. J. Manninen, Springer Proceedings in Physics Vol. **48** (Springer, New York, 1990), p. 64.
[79]D. G. Pettifor and I. I. Oleinik, Phys. Rev. B **59**, 8487 (1999).
[80]D. G. Pettifor and I. I. Oleinik, Phys. Rev. Lett. **84**, 4124 (2000).
[81]D. G. Pettifor and I. I. Oleinik, Phys. Rev. B **65**, 172103 (2002).
[82]R. Drautz, D. Nguyen-Manh, D. A. Murdick, X. W. Zhou, H. N. G. Wadley, and D. G. Pettifor, TMS Lett. **1**, 31 (2004).
[83]R. Drautz, D. A. Murdick, D. Nguyen-Manh, X. W. Zhou, H. N. G. Wadley, and D. G. Pettifor, Phys. Rev. B **72**, 144105 (2005).
[84]J. Nord, K. Albe, P. Erhart, and K. Nordlund, J. Phys. Condens. Matter **15**, 5649 (2003).
[85]K. Albe, K. Nordlund, J. Nord, and A. Kuronen, Phys. Rev. B **66**, 035205 (2002).
[86]X. W. Zhou, D. A. Murdick, B. Gillespie, and H. N. G. Wadley, Phys. Rev. B **73**, 45337 (2006).
[87]D. A. Murdick, X. W. Zhou, H. N. G. Wadley, R. Drautz, and D. G. Pettifor, Mater. Res. Soc. Symp. Proc. E **859**, JJ9.7.1 (2005).
[88]D. A. Murdick, H. N. G. Wadley, and X. W. Zhou, Phys. Rev. B **75**, 125318 (2007).
[89]D. K. Ward, X. W. Zhou, B. M. Wong, and F. P. Doty, "Analytic bond-order potential for cadmium telluride system," (unpublished).
[90]I. Barin, O. Knacke, and O. Kubaschewski, *Thermochemical Properties of Inorganic Compounds* (Springer-Verlag, Berlin, 1977).
[91]R. Viswanathan, M. Sai Baba, D. Darwin Albert Raj, R. Balasubramanian, T. S. Lakshmi Narasimhan, and C. K. Mathews, Spectrochimica Acta B **49**, 243 (1994).
[92]V. Lukeš, M. Ilčin, V. Laurinc, and S. Biskupič, Chem. Phys. Lett. **424**, 199 (2006).
[93]K. P. Hube and G. Herzberg, *Molecular Spectra and Molecular Structure. IV. Constants for Diatomic Molecules* (Van Nostrand Reinghold, New York, 1979).
[94]J. M. Rowe, R. M. Nicklow, D. L. Price, and K. Zanio, Phys. Rev. B **10**, 671 (1974).
[95]A. Béré, J. Chen, A. Hairie, G. Nouet, and E. Paumier, Comput. Mater. Sci. **17**, 249 (2000).
[96]G. Parthasarathy and W. B. Holzapfel, Phys. Rev. B **37**, 8499 (1988).
[97]J. Hafner, J. Comput. Chem. **29**, 2044 (2008).
[98]J. P. Perdew, K. Burke, and M. Ernzerhof, Phys. Rev. Lett. **77**, 3865 (1996).